A&A 470, 73–81 (2007)
DOI: 10.1051/0004-6361:20066248

Astronomy & Astrophysics

An X-ray look at the Seyfert 1 Galaxy Mrk 590: *XMM-Newton* and *Chandra* reveal complexity in circumnuclear gas

A. L. Longinotti[1], S. Bianchi[1], M. Santos-Lleo[1], P. Rodrìguez-Pascual[1], M. Guainazzi[1], M. Cardaci[1,2], and A. M. T. Pollock[1]

[1] European Space Astronomy Centre, Apartado 50727, 28080 Madrid, Spain
[2] Departamento de Física Teórica, C-XI, Universidad Autónoma de Madrid, 28049 Madrid, Spain
e-mail: alonginotti@sciops.esa.int

Received 14 August 2006 / Accepted 8 January 2007

ABSTRACT

Context. This paper reports on a partially simultaneous observation of the bright Seyfert 1 Galaxy Mrk 590, performed by XMM-Newton and Chandra.
Aims. The long exposure (∼100 ks) allows us to investigate the Fe K complex at 6−7 keV and the presence of soft X-ray spectral features in great detail.
Methods. We have analysed XMM-Newton data from the European Photon Imaging Camera (EPIC) in the 0.5−12 keV band and from the Reflection Grating Spectrometer (RGS) in the 0.35−2.5 keV band, and data from the High Energy Transmission Gratings (HETGs) onboard Chandra. UV and optical data from the Optical Monitor (OM) onboard XMM-Newton are also included in the analysis.
Results. The broad band spectrum is well described by an unabsorbed power law and three unresolved Fe K lines in the 6−7 keV range. The presence of a Compton reflection component and a narrow Fe K line at 6.4 keV is consistent with an origin via torus reflection. The ionised Fe lines at ∼6.7 and 7 keV are instead most likely originated by scattering on a warm and ionised gas. The soft X-ray spectrum appears to be almost featureless due to the very bright continuum emission, except for one emission line identified as OVIII Lyα detected at ∼19 Å by both RGS and Chandra-MEG. The emerging picture consists of an active nucleus seen directly on a "clean" line of sight without intervening material, surrounded by photoionised circumnuclear gas at a high ionisation level. We also study three serendipitous sources in the field of view of Chandra and XMM-Newton. One of these sources may be identified with an ULX of $L_{0.3-10\ \mathrm{keV}} \sim 4 \times 10^{40}$ erg/s.

Key words. galaxies: active – galaxies: individual: Mrk 590 – line: profiles

1. Introduction

Active galactic nuclei (AGN) have been observed in the X-ray domain for many years. Nowadays, it is fair to say that the overall spectral shape of Seyfert 1 Galaxies is quite well known. The hard X-ray continuum (2−10 keV) is well described by a power law produced by Inverse Compton scattering (Haardt & Maraschi 1993) with average photon index $\Gamma \sim 1.9$ (Piconcelli et al. 2005). The extrapolation of the power law to lower energies in some cases implies an excess in soft X-ray emission; in many sources the soft X-ray spectrum is affected by absorption or emission features originated in a photoionised medium along the line of sight (Kaastra et al. 2000; Kaspi et al. 2001).

Reflection of X-ray photons by optically thick material may also occur and in this case it gives rise to a hard X-ray Compton reflection component and prominent Fe K features (George & Fabian 1991). The properties of Fe K features can provide much information on the origin of the X-ray emitting gas. In the case of reflection by an accretion disc, the Fe line profile is relativistically broadened and skewed (Fabian et al. 2000). When X-ray photons are reflected by distant material, like the torus proposed in the unification scheme (Antonucci 1993; Ghisellini et al. 1994), the resulting profile is narrow and, in most cases, unresolved by the current instrumentation. Since Fe K lines could also be produced in the broad line region (BLR) in an analogous way to the broad UV/Optical lines, a contribution of the BLR emission to the cores of narrow Fe lines cannot be excluded (Yaqoob & Padmanabhan 2004; Nandra 2006).

What is as yet unclear is which scenario is the most common in Sy1 Galaxies. Recent observations with *XMM-Newton* and *Chandra* have shown that a narrow Fe K line is an almost ubiquitous component of the X-ray spectra of type 1 AGNs (Yaqoob & Padmanabhan 2004; Jimenez-Bailon et al. 2005). On the other hand, only a handful of sources seem to host a relativistically broadened diskline (Nandra et al. 1999; Turner et al. 2002; Ponti et al. 2002; Longinotti et al. 2003).

Mrk 590 ($z = 0.026$) is a bright Seyfert 1 galaxy. It was observed by the *Einstein* observatory (Kriss et al. 1980) and by HEAO 1 as part of the Piccinotti sample (Piccinotti et al. 1982). *Exosat* data of Mrk 590 did not reveal any particular spectral complexity (Turner & Pounds 1989). More recently, it was detected in the high-energy domain by *BATSE*, in the 20−200 keV band (Malizia et al. 1999). Despite being part of one of the best studied AGN samples (the Piccinotti's), Mrk 590 has not been observed by *ASCA* or by *BeppoSAX*. Therefore, the hard X-ray spectral properties of this AGN have remained almost unknown until the analysis of a 10 ks *XMM-Newton* observation was reported by Gallo et al. (2006). In this work, the 0.3−10 keV flux was reported to be about 8.4×10^{-12} erg cm^{-2} s^{-1}, the 2−10 keV luminosity was 0.7×10^{43} erg s^{-1} and the presence of a strong Fe K line was revealed in the EPIC data. Here we will discuss

Table 1. Observation log. Mrk 590 was observed by *Chandra* on July 3rd, 2004 and by *XMM-Newton* on the following day. A simultaneous exposure of 65 ks was obtained.

Satellite	Instrument	Exposure	Flux_{2-8}
–	–	(ks)	(10^{-12} erg cm^{-2} s^{-1})
Chandra	HETG	95	$6.72^{+0.38}_{-0.45}$
XMM-Newton	EPIC/pn	71	5.62 ± 0.09
	EPIC/MOS1	85	5.97 ± 0.09
	EPIC/MOS2	90	5.60 ± 0.09
	RGS	105	–

a quasi simultaneous observation of this source performed by *XMM-Newton* and *Chandra* for about 100 ks.

2. Observation and data reduction

2.1. The XMM-Newton data

Mrk 590 was observed by *XMM-Newton* on July 4, 2004 (OBSID 0201020201). Data from the EPIC, RGS and OM instruments were available (Struder et al. 2001; Den Herder et al. 2001; Mason et al. 2001). The nominal duration time was 100 ks. The observation was performed in Small Window mode for the pn and the MOS1 cameras, while the MOS2 was operated in Full Frame. The raw data were processed with SAS 6.5.0 with the tasks `epchain` for the pn data and `emchain` for the MOS data. During the satellite operation, the scheduled observation was stopped for about 15 min due to telemetry loss, so that two distinct event lists were obtained for each detector. These two event files were then merged in one file by running the SAS task `merge` (Gabriel et al. 2004). Screening for flaring background due to high-energy particles was applied to this final event list. Intervals affected by background flares were removed by selecting events with a count rate lower than 0.6 cts/s in the 10−12 keV light curve. Source and background counts were extracted from circular regions of 40 arcsec. No pile-up affects the observation, as tested with the task `epatplot`, so that patterns 0 to 4 were selected for the pn spectra and patterns 0 to 12 were selected for the MOS ones. The effective exposures times are 71, 85 and 90 ks, respectively for the pn, MOS1 and MOS2 (see Table 1). Because of the different observing modes of the MOS data, it was not possible to co-add the spectra and therefore they are kept and analysed separately. Spectra were grouped to have 100 counts/bin for the pn data and 50 counts/bin for the MOS. Response matrices were created employing the SAS tasks `arfgen` and `rmfgen` for EPIC data.

RGS data were processed with the task `rgsproc`, yielding a useful exposure time of 105 ks. A response matrix was created for the spectral analysis by the task `rgsrmfgen`. No binning is applied to the RGS spectra. The data from the Optical Monitor were reduced running the task `omichain`.

During the *XMM-Newton* observation, the source did not vary significantly in flux and it did not show spectral variations. The light curves of the pn data plotted in Fig. 1 do not reveal any particular temporal behaviour. Therefore, the spectral analysis described in the following Sects. is performed on the integrated spectrum.

2.2. The Chandra data

Mrk 590 was observed by *Chandra* HETG (High Energy Transmission Gratings: Canizares et al. 2005) in July 2004 for about 100 ks. The *Chandra HETGS* consists of two assemblies, the High Energy Grating (HEG) in the 0.8−10 keV, and the Medium Energy Grating (MEG), in the 0.4−5 keV. Data were reduced with the Chandra Interactive Analysis of Observations (CIAO) 3.2.1 and the Chandra Calibration Database (CALDB) 3.0.1, adopting standard procedures. In particular, a new evt2 file was created with `acis_process_events`, adopting an observation-specific bad pixel file and reconstructing the grating extraction region and events with `tgdetect`, `tg_create_mask` and `tg_resolve_events`. An exam of the light curve confirms that no variability is observed during the Chandra exposure, as already emerged for the *XMM-Newton* data. First-order HEG and MEG spectra were extracted with `tgextract` and then co-added with `add_grating_orders`. In the following analysis, we binned the spectra at the resolution of the instruments, i.e. 0.012 and 0.023 Å (*FWHM*), for HEG and MEG, respectively. The C-statistic was employed in the spectral fitting and all statistical errors are given at 90% level of confidence ($\Delta C = 2.71$).

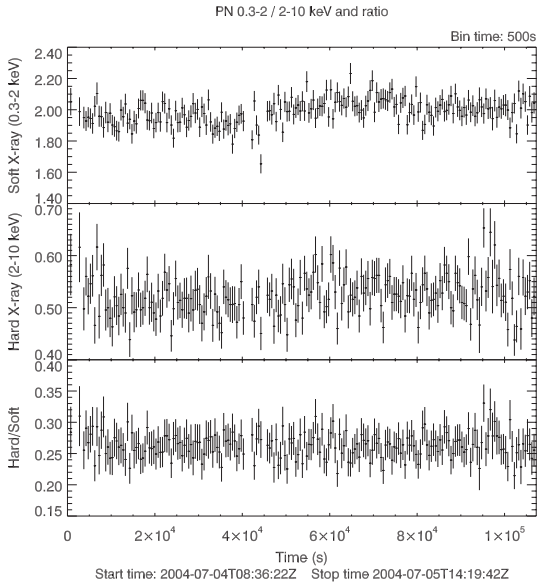

Fig. 1. Light curves of the EPIC/pn data in the soft X-ray band (*top*), hard X-ray band (*medium*) and their hardness ratio (*bottom*). The background-subtracted count rates are plotted. The source does not show variability.

3. Spectral analysis

3.1. XMM-Newton/EPIC spectra

Galactic absorption of column density $N_{\rm H} = 2.7 \times 10^{20}$ cm^{-2} is included in all the following spectral fits (Dickey & Lockman 1990). Errors are quoted at the 90% confidence level for one interesting parameter (i.e. $\Delta\chi^2 = 2.71$). Throughout the text, the energies are quoted in the source frame and the adopted cosmological constant is $H_0 = 70$ km s^{-1} Mpc^{-1}. The measured flux and luminosity in the soft and hard X-ray bands are: $F_{0.3-2\ \rm keV} \sim 4.4 \times 10^{-12}$ erg cm^{-2} s^{-1}, $L_{0.3-2\ \rm keV} \sim 0.67 \times 10^{43}$ erg s^{-1} and $F_{2-10\ \rm keV} \sim 6.4 \times 10^{-12}$ erg cm^{-2} s^{-1}, $L_{2-10\ \rm keV} \sim 0.97 \times 10^{43}$ erg s^{-1}.

When the EPIC spectrum is fitted in the 0.5−12 keV energy range with a simple power- law model, the residuals clearly reveal strong emission in the Fe K complex and emission in excess in the hard X-ray continuum (Fig. 2). The energy range

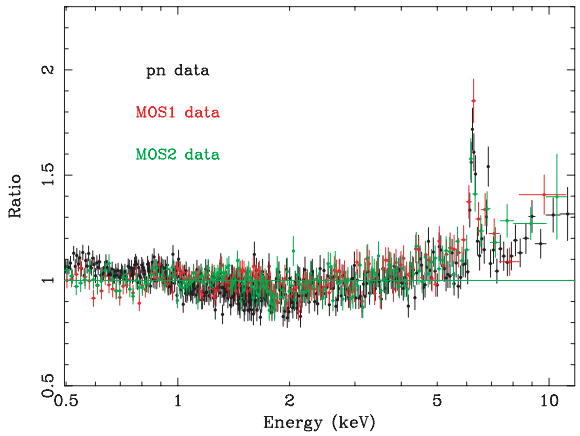

Fig. 2. Ratio of the broad band spectrum fitted by a power law with $\Gamma \sim 1.76$. The residuals above 5 keV are evident (source frame plot).

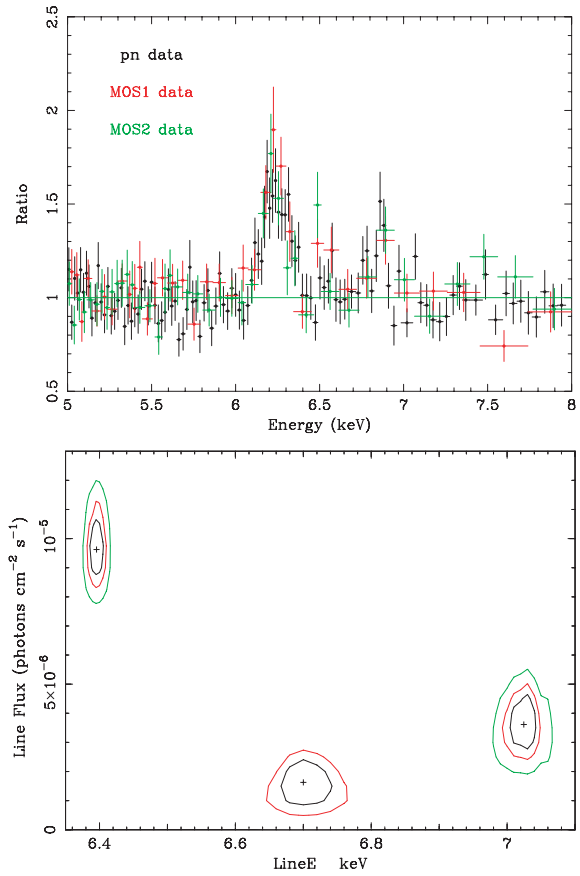

Fig. 3. *Top panel*: the ratio of the EPIC data fitted by a power law shows three emission lines corresponding to Fe K transitions at ∼6.4, 6.7 and 7 keV (source frame plot). *Bottom panel*: confidence contours at 68.3, 90 and 99% levels of confidence for the energy and intensity of the 3 lines. All the three lines have unresolved width. The line at 6.7 keV is less significant than the other two and this is why only two contours are shown (68.3 and 90%).

has therefore been restricted to the 2−12 keV band in order to investigate this region of the spectrum. Fitting the data with a power law of photon index ∼1.6 yields an unacceptable fit (χ^2/d.o.f. = 1209/971). A zoom of the ratio of the hard X-ray data to a power-law model is shown in the top panel of Fig. 3: three emission lines are clearly seen in all the three detectors in the ∼6−7 keV range. Three Gaussian emission lines were added,

Table 2. Fe K lines parameters in the 2−12 keV best-fitting model of the EPIC data. Energies are rest-frame, the photon index is $\Gamma = 1.62^{+0.02}_{-0.02}$.

EPIC 2−12 keV best-fit: plaw+3 zgauss				
$E_{\rm Line}$ (keV)	σ (eV)	EW (eV)	Flux ($\times 10^{-6}$ ph cm^{-2}s^{-1})	χ^2/d.o.f.
$6.39^{+0.02}_{-0.02}$	36^{+18}_{-24}	121^{+11}_{-16}	9.62 ± 1.07	948/964
$7.02^{+0.02}_{-0.02}$	<57	52^{+15}_{-12}	$3.61^{+1.02}_{-0.89}$	-
$6.70^{+0.04}_{-0.04}$	<85	18^{+10}_{-10}	$1.61^{+0.88}_{-0.94}$	-

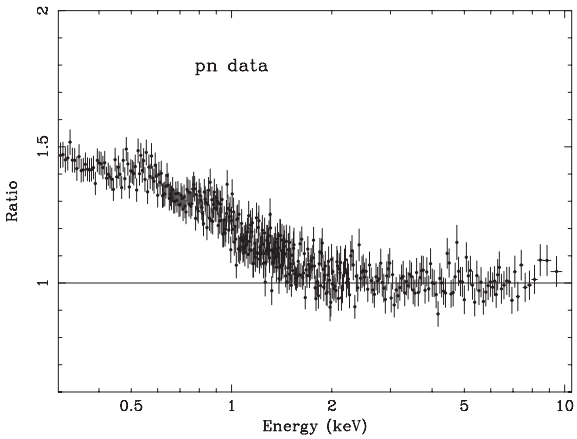

Fig. 4. Data-to-model ratio of the pn spectrum fitted with the hard X-ray best fit in Table 2. The presence of a soft X-ray component is evident in the figure.

initially with width free to vary. The best-fitting lines parameters are summarised in Table 2. Adding a 6.4 keV line yields an improvement in $\Delta\chi^2 = 215$, for 3 d.o.f. The line width can be constrained for this line to $\sigma = 36^{+18}_{-24}$ eV. A second line at 7.02 ± 0.02 keV improves the fit of $\Delta\chi^2 = 36$, for 2 d.o.f. with an upper limit on the line width of $\sigma < 57$ eV. The width is thus kept fixed to 1 eV. A third line is detected with lower significance at ∼6.7 keV with an upper limit on the width of 85 eV ($\Delta\chi^2 = 10$ for 2 d.o.f.). The line width is kept fixed to 1 eV, as for the previous case. The confidence contours for these three lines are plotted in the bottom panel of Fig. 3.

In the following, we analyse the spectrum over the entire energy range using the pn data only, since adding the MOS does not yield a relevant improvement for the analysis of the continuum. Nonetheless the MOS have been checked and they are confirmed to be consistent with the pn results. The power law+3 Gaussian lines fit extended to the full energy range is not satisfactory (χ^2/d.o.f. = 1173/750): the presence of a soft X-ray component is clear when the data below 2 keV are taken into account (Fig. 4). The data were checked for the presence of Compton reflection since the narrow neutral Fe K line is likely to be originated via reflection onto optically thick matter and the residuals still present above ∼5−6 keV indicate that this may be the case. A PEXRAV component (Magdziarz & Zdziarski 1995) with an inclination angle fixed to 30° was thus added to the model. The reflection parameter is defined as $R = \Omega/2\pi$ with $R \sim 1$ if the reprocessing material covers 2π of the source. The addition of the reflection component improves the χ^2 considerably (χ^2/d.o.f. = 811/749), but the fit yields an extremely high reflection fraction, $R \sim 3.6$, and unsatisfactory residuals in the soft X-ray band. We have then tested for the presence of two additional components, i.e. absorption and blackbody emission. No absorption seems to be required by the data and in fact

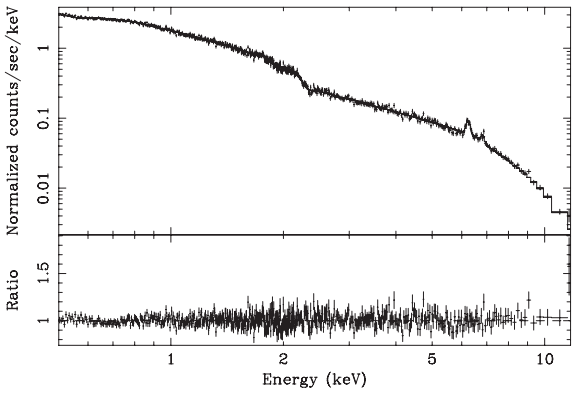

Fig. 5. Spectrum and ratio of the pn data fitted with the best-fitting model (power law, three Fe K emission lines, reflection component and blackbody).

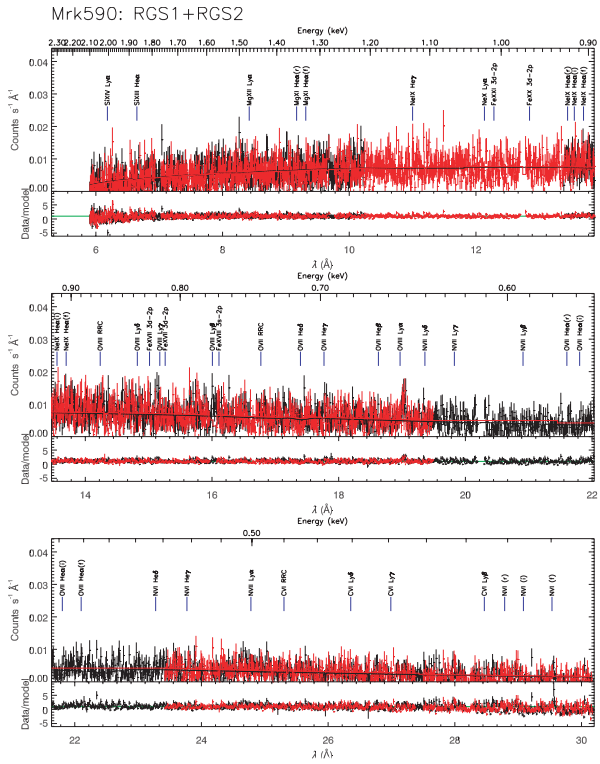

Fig. 6. The plot shows the RGS1 (black) and RGS2 (red) spectrum and the residuals of the data fitted with Galactic absorption and the best-fitting power law with photon index $\Gamma = 1.68 \pm 0.03$. The only prominent line is the OVIII Lyα around 19 Å. This figure has been produced reprocessing the data with SAS 7.0.0 due to the better calibrations.

neither cold nor warm absorber models improve significantly the fit (respectively, models WABS and ABSORI in XSPEC). Adding a blackbody component instead yields χ^2/d.o.f. = 762/747, with best-fitting parameters $\Gamma = 1.73^{+0.03}_{-0.03}$, $R = 1.3^{+0.7}_{-0.6}$ and blackbody temperature $kT = 156^{+14}_{-12}$ eV. We note that the blackbody parameters are in good agreement with the results from Gallo et al. (2006). The spectrum fitted with this model and the resulting residuals are plotted in Fig. 5. The description of the soft excess with a blackbody model is somewhat unsatisfactory. The issue of finding a physical explanation for the soft excess represents a well known problem in AGNs studies (e.g. Gierlinski & Done 2004). It has been shown in fact that the majority of Active Nuclei are characterised by the same temperature ($kT \sim 0.1$ keV, see Piconcelli et al. 2005; Crummy et al. 2006) when their soft X-ray spectra are fitted with a blackbody model. This is in contradiction with the prediction that the blackbody spectrum emitted by an accretion disc associated with a supermassive black hole emits at a much lower temperature (i.e. ~tens of eV). Alternative models have been tried in the following. A broken power law with break energy around 1.9−2 keV and with $\Gamma_{\rm soft} = 1.89 \pm 0.01$ and $\Gamma_{\rm hard} = 1.62 \pm 0.01$ yields a slightly better fit (χ^2/d.o.f. = 758/746). This implies that the shape of the soft X-ray spectrum is not compatible only with a blackbody spectrum. Recently, the REFLION model (Ross & Fabian 2005) has been successfully employed to fit the soft excess in AGN providing that relativistic blurring is applied to the spectrum (Crummy et al. 2006). The presence of the ionised Fe lines may suggest an origin in an ionised accretion disc, although there is no evidence of relativistic effects in Mrk 590, mainly because the Fe lines profiles are found to be narrow. We have tested REFLION with a power law and a narrow Gaussian line at 6.4 keV (which would not be calculated by the photoionised disc code). This model does not improve the fit statistic (χ^2/d.o.f. = 793/750) nor it does provide a good fit to the ionised lines. We conclude that an ionised reflection and a disc origin for the ionised Fe lines can be excluded in this case.

3.2. XMM-Newton/RGS spectra

The absence of intrinsic absorption in the soft X-ray spectrum emerged through the analysis of the EPIC data, is confirmed by looking at the RGS spectrum (Fig. 6). Indeed, no obvious emission or absorption features are visible above the noise, except for the OVIII Lyα at ~19 Å. The unbinned spectrum was therefore analysed with XSPEC in a small wavelength range around this emission line with the aim to perform a "local" fit. The C-statistic (Cash 1976) was applied because some energy bins may fall in the limit of a few number of counts. Statistical errors are given at a 90% level of confidence ($\Delta C = 2.71$). The ratio of the data in the ~18−20 Å to a model consisting of a power law and the Galactic absorption, is plotted in Fig. 7: a narrow line is evident in the data. When the line is fitted with a 0-width Gaussian profile, it is detected at $\lambda = 19.02 \pm 0.01$ Å with $\Delta C = 25.5$ for 2 d.o.f. The flux is $1.06^{+0.43}_{-0.48} \times 10^{-5}$ photons cm^{-2} s^{-1}. The line appears to be emitted with some not negligible shift ($\sim\Delta\lambda = 0.060$ Å) with respect to the rest wavelength of the OVIII Lyα i.e. $\lambda = 18.96$ Å.

We have checked the spectrum for the presence of similar shifts in other emission features, but the X-ray continuum is so intense that it may well hamper the detections of other line complexes. The only emission structure that may be strong enough to be detected is the OVII triplet at ~22 Å (see Fig. 6). Unfortunately, only the RGS1 data are available in this wavelength range due to the electronic chain failure of CCD 4 in the RGS2. The upper limits on the intensity of two lines in the triplet could be obtained: for the lines at 21.60 Å and 22.10 Å, they are respectively 1.16×10^{-5} and 2.05×10^{-5} photons cm^{-2} s^{-1}, but no information on the lines' positions can be gained. Thus, we cannot confirm if the shift in the wavelength peak of the OVIII line is common to other features in the RGS.

3.3. The Chandra/HETGs spectra

The HEG spectrum was fitted in the hard X-ray band by a power law with $\Gamma = 1.68^{+0.10}_{-0.08}$, consistent with the value found in the

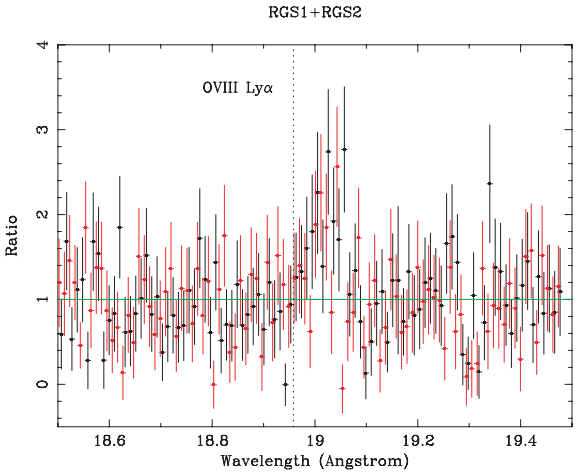

Fig. 7. Ratio of the RGS data to a power-law model in the 18.5−19.5 Å (corrected for the redshift of the source). The emission line at ∼19 Å is evident in both RGS1 (black points) and RGS2 (red points). The dashed line marks the OVIII Lyα rest frame wavelength.

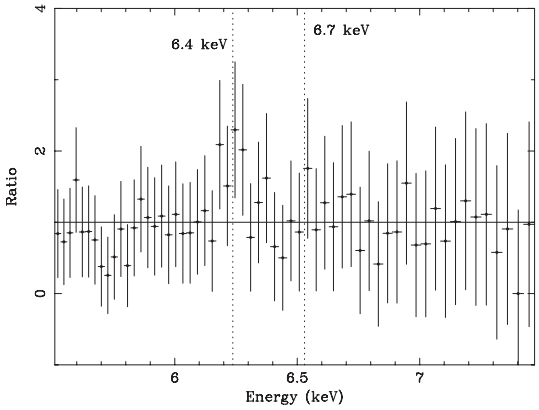

Fig. 8. Ratio of the Chandra HEG data to a power-law model (plotted in the source frame).

XMM-Newton data. The ratio of the data to a power law model in the 5−8 keV is plotted in Fig. 8. Only 190 counts are present in the 6−7 keV range.

We checked for the presence of the Fe K lines detected in the EPIC spectra. Adding a narrow line at 6.4 keV improves the fit by $\Delta C = 22$ (for 3 d.o.f.). The parameters of the line are consistent with the results in Sect. 3.1 from the EPIC data. For the neutral line $E = 6.40^{+0.04}_{-0.03}$ keV, $\sigma = 47^{+58}_{-24}$ eV and $EW = 160^{+118}_{-78}$ eV. The line flux is found to be $1.5^{+1.1}_{-0.7} \times 10^{-5}$ photons cm^{-2} s^{-1}. Adding another Gaussian with unresolved width at ∼6.7 keV does not improve the fit very significantly ($\Delta C = 3$, for 2 d.o.f.), in fact only the upper limit on the line intensity was found (7.8×10^{-5} photons cm^{-2} s^{-1}). No line is detected at higher energies, but the upper limit on the flux and corresponding EW for a narrow line at 7.0 keV (respectively 2.5×10^{-6} photons cm^{-2} s^{-1} and 30 eV) are consistent with the results from *XMM-Newton*.

In the lower energy band, the MEG spectrum was searched for the presence of spectral lines, although the intense continuum would make their detection rather difficult, as was already pointed out for the RGS data (Sect. 3.2). We concentrate in particular on the range 18−20 Å with the intent of confirming if the ∼19 Å line is observed with the same shift as it was in the RGS. We have performed a local fit as done for RGS, employing C-statistic and fitting a zero-width Gaussian line in a narrow band around the expected emission wavelength. The line is actually present in the MEG data and it is detected with $\Delta C = 16.5$ at a wavelength thoroughly consistent with the rest-frame position: $\lambda = 18.97 \pm 0.01$ Å. The observed flux is $2.10^{+1.48}_{-1.19} \times 10^{-5}$ photons cm^{-2} s^{-1}. No other feature was found in the MEG spectrum.

The difference between the peak wavelength of the line observed in the RGS spectrum and in the MEG spectrum is not negligible ($\sim\Delta\lambda = 0.060$ Å). We investigate the reasons for the discrepancy in the following. As reported in Table 1 the *XMM-Newton* and *Chandra* observations are not exactly simultaneous, but they overlap for a total time of about 65 ks. Therefore, it was first checked if the discordancy found in the RGS and MEG data concerning the detection of the emission line at ∼19 Å could be due to variability intrinsic to the source. The RGS spectrum was extracted from the portion of time when both satellites were operative, yielding an exposure of 58 ks. After repeating the analysis of the line using these data, no change in the line position is found, so it is very unlikely that the two measurements disagree for physical reasons related to source variability.

An error in the choice of the source coordinates may introduce a systematic error in the wavelength assigned to each photon of the source spectrum; in our case the RGS data were processed inputting the coordinates corresponding to the optical nucleus of Mrk 590, so we tend to exclude that the spectrum was shifted due to an erroneous choice of the source position occurring during the data reduction. We have checked if this same problem may have occurred in the Chandra data. In fact if the zero-order image in the Grating event list is piled up, it may lead to an incorrect wavelength scale[1]. Our observation was not affected by this issue. Once the goodness of the line position in Chandra is assured, it seems reasonable not to question it, simply because the line is detected at the rest wavelength, i.e. where it is expected.

The systematic errors in the wavelength scale in the RGS are of the order of 20 mÅ. The difference between the laboratory and the measured wavelengths in a set of certain emission lines is generally around this value, but it may be larger for some individual measurements[2]. We conclude that the shift in the RGS is probably due to instrumental effects because an atypical error in the wavelength occurred in this observation.

3.4. XMM-Newton: optical monitor data

The fluxes from the Optical Monitor were obtained in five bands: B, U, $UVW1$, $UVM2$ and $UVW2$ (see Table 3). These values were estimated by converting the mean count rates in each OM filter, according to the guidelines provided in the SAS documentation. They have been corrected for extinction assuming the extinction law by Cardelli et al. (1989). The images in the B- and U-bands could not be used to estimate the contribution of the galaxy in these filters because of instrumental artifacts. Nonetheless, it was possible to ascertain the presence of extended emission in these two images. We have fitted a 2-dimensional Gaussian to the brightest (point-like) sources in

[1] See http://cxc.harvard.edu/ciao3.3/threads/tg_piled_zero/

[2] http://xmm.vilspa.esa.es/external/xmm_user_support/documentation/uhb/node54.html

Table 3. Fluxes obtained from the Optical Monitor data. These values are corrected for the Galactic extinction.

Filter	λ	Flux
–	(Å)	($\times 10^{-15}$ erg cm^{-2} s^{-1}Å^{-1})
B	4500	5.76 ± 0.01
U	3440	2.97 ± 0.01
$UVW1$	2910	2.46 ± 0.02
$UVM2$	2310	2.49 ± 0.07
$UVW2$	2120	1.97 ± 0.10

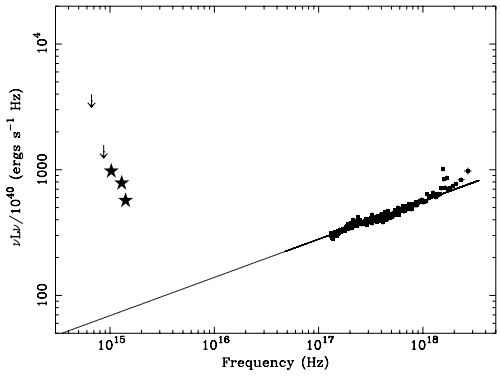

Fig. 9. Spectral energy distribution including the X-ray and UV-optical data, with the extrapolation of the best fit X-ray power law. The luminosity in the y-axis is in units of 10^{40} erg/s. The points marked as upper limits are the U- and B-band points, where the contribution of the host galaxy has not been subtracted. The points marked as stars are the other UV fluxes obtained by the OM.

the field of view and to Mrk 590. This is in general a good model to fit emission from a point-like source, but it is not appropriate for modeling extended emission. From the comparison of the fits, it was possible to say that in the B and U filters Mrk 590 was not as well fitted as the other point-like sources. This is due to the fact that the source must be more extended and therefore we can say that the contribution of the host galaxy is not negligible in the B- and U-bands. In the $UVW1$ filter the image shows that the emission is concentrated in the nucleus rather than in the galaxy and in the other filters the contribution from the active nucleus is clearly predominant.

The spectral energy distribution was constructed by taking the OM fluxes and the X-ray data points in the 0.5−12 keV (Fig. 9). The points in the U- and B-bands are marked as upper limits to highlight that the contribution of the host galaxy, although estimated qualitatively, is not negligible. The fluxes measured in the optical/UV are located above the extrapolation of the X-ray power law, indicating the presence of a UV bump. It is nonetheless quite difficult to relate the shape of this component to the soft X-ray spectrum due to the Galactic absorption between the two bands. To clarify the relation between the emission in the optical/UV and X-ray band, the index $\alpha_{\rm ox}$ defined as the slope of a power law extending between 2500 Å and 2 keV rest frame can be used as a good indicator of the "X-ray loudness" of an AGN. The definition $\alpha_{\rm ox} = -0.3838 \log[F\nu(2\,{\rm keV})/F\nu(2500\,{\rm Å})]$ reported by Strateva and collaborators (2005) was adapted with the flux at 2310 Å to replace the UV flux in the ratio. This change would not affect the results because the fluxes at 2310 and 2910 Å differ by a few percent (see Table 3). The $\alpha_{\rm ox}$ calculated in this way is found to be −0.88, slightly larger than the value found for the objects studied by Strateva et al. (2005), but still typical for Seyfert 1 galaxies.

4. Discussion

4.1. The hard X-ray spectrum and the Fe K lines

The 6.4 keV Fe K line detected by both observatories in Mrk 590 appears too narrow to be produced in the inner accretion disc, otherwise its profile would be distorted and broadened by the black hole gravity. Consequently, the line producing material has to be situated in outer regions far away from the nucleus. One viable interpretation is that the line is originated via Compton reflection onto the torus-shaped material distributed at a large distance from the central source according to the AGN unification models (Ghisellini et al. 1994). The reflection fraction determined in our best-fitting model and the EW of the 6.4 keV line are in quite good agreement with the predictions of George & Fabian (1991) for reflection on optically thick matter. The results from the spectral fit in Sect. 3.1 therefore concur to suggest that the hard X-ray spectrum arises from reprocessing on the torus.

Another possible explanation for the Fe K line could be emission in the broad-line emitting gas. The extremely good quality of the *XMM-Newton* spectrum combined with the *Chandra* grating allowed us to measure the width of the Fe K line in this source. The two measurements are in good agreement ($\sigma = 36^{+18}_{-24}$ eV in EPIC and $\sigma = 47^{+58}_{-24}$ eV in the HEG data), corresponding to a $FWHM$ of 4000^{+2000}_{-2700} km s^{-1} and 5250^{+6500}_{-2700} km s^{-1}, respectively. The $FWHM$ of the Hα line in Mrk 590 is reported to be ∼2400 km s^{-1} (Stirpe 1990), implying that this source is actually much closer to the Narrow Line Sy 1 class (Boller et al. 1996), at least with respect to the optical lines' properties. Unfortunately, this means that regardless of resolving the Fe Kα line width as done herein, it is somewhat difficult to ascertain if the line comes from the BLR because the width of the BLR lines in Mrk 590 is smaller than in the typical Sy1 case. The torus hypothesis, corroborated by the presence of the neutral reflection component in the spectrum, remains therefore the favoured scenario for the production of the Fe K line.

The two lines emitted at ∼6.7 and ∼7 keV are fully consistent with emission from Fe XXV (6.7 keV) and XXVI (6.96 keV), therefore from iron in a very ionised state. A contribution of the Kβ from neutral Fe to the Fe XXVI line cannot be ruled out by these data. The centroid energy of the line is in fact slightly higher (∼7.02 keV) than would be expected for Fe XXVI only. The 7 keV line is not detected in Chandra and the addition of a Kβ component in the EPIC best fit (Table 2) was not significant. Nevertheless, it is possible to obtain a qualitative estimate of the contribution of the Kβ to the XXVI Fe line taking into account the flux ratio Fe Kβ/Fe Kα, which has been calculated to be around 0.15 for neutral iron (see Molendi et al. 2003). Referring to this value, we have included a fourth Gaussian line to the best fit reported in Table 2 with energy fixed to 7.06 keV and intensity fixed to 1.34×10^{-6} photons cm^{-2} s^{-1}, i.e. the energy and the estimated Fe Kβ flux. In this way, the Fe XXVI line flux decreases to $2.44^{+0.94}_{-0.95} \times 10^{-6}$ photons cm^{-2} s^{-1}, corresponding to ∼35 eV. Ionised iron lines with EW of tens of eV against the total continuum can be produced by fluorescence and scattering in a photoionised medium out of the line of sight, not only in Seyfert 1 objects as NGC 7213 (Bianchi et al. 2003a) and NGC 5506 (Bianchi et al. 2003b), but also in many Seyfert 2 cases (Bianchi et al. 2005, and references therein). The *Chandra*

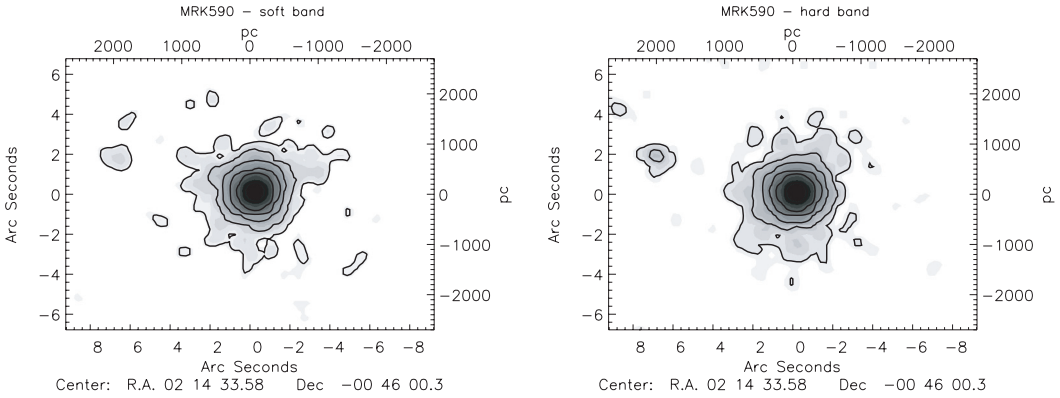

Fig. 10. *Chandra* images of Mrk 590 in the 0.3−2 keV band (*left*) and in the 2−10 keV band (*right*) with contour levels of the emission superimposed. The source visible to the west of the nucleus of the AGN (Source A in this paper) is discussed in Sect. 5.

images in Fig. 10 tentatively show that the X-ray emission may be extended on a kpc scale. The ionised lines may be be originated in this extended gas, which is not otherwise observable in the spectrum due to the intensity of the primary nuclear continuum. The results obtained from the analysis of the hard X-ray spectrum do not provide any particular evidence for any accretion disc signature, in agreement with many observations of type 1 AGNs (Bianchi et al. 2004; Matt et al. 2006).

4.2. The soft X-ray spectrum

As mentioned in Sect. 3.1, the spectrum of Mkn 590 is not absorbed, making this source fall into the fraction of Sy1 Galaxies (∼50%) that do not show intrinsic absorption (Reynolds 1997; George et al. 1998). The only relevant feature observed in the high resolution spectra is the O VIII Lyα emission line. Most probably, the line arises by photoionisation processes in warm gas. Netzer et al. (2005) provided photoionisation calculations of line ratios for the case of the starburst galaxy NGC 6240. Among these, the intensities of the Fe XXV and XXVI lines relative to the OVIII Lyα were estimated (the line fluxes were quoted in units of erg cm^{-2} s^{-1}). Using the same units, the line ratios FeXXV/OVIII and FeXXVI/OVIII in our data are estimated around 1.6 and 1.3 (this last value is approximated because an exact estimate of the line flux is affected by the presence of the FeKβ). A qualitative comparison with Netzer's (2005) results shows that it is possible to have photoionised gas producing OVIII Lyα and strong Fe XXV and XXVI lines with these ratios, providing that the gas is characterised by a rather high value of the ionisation parameter, i.e. $U > 2$, where U is defined as the photon to hydrogen density ratio in the range 0.54−10 keV. Of course, this cannot exclude a priori the more realistic picture of a multi-phase medium with various ionisation parameters. Likewise, the apparent lack of features from other transitions in the soft X-ray spectrum may indicate that the material is highly photoionised, but this is a tentative conclusion since we are unsure about the detection of other lines in the RGS spectrum (e.g. the OVII triplet, Sect. 3.2).

Most of the Seyfert 1 galaxies with narrow emission lines in RGS spectra are also characterised by the presence of warm absorbers: for example the OVIII Lyα emission line has been observed in NGC 3783 (Behar et al. 2003), NGC 7469 (Blustin et al. 2003) and Mrk 509 (Smith et al. 2006). Particularly, in the case of NGC 3783 it was suggested to relate the X-ray absorbing gas to the OVIII line-emitting plasma. Mrk 590 represents a peculiar case because of the absence of warm absorption and of the presence of X-ray emission lines from highly ionised elements at once. We can try to explain the unusual spectrum of this galaxy with simple considerations. The soft X-ray spectrum appears to be made by an intense nuclear component with a mild contribution of a photoionised medium probably in different ionisation phases revealed by the observation of highly ionised O and Fe lines. The characteristics of this medium resemble those found in Seyfert 2 objects, where the soft X-ray spectrum is due to photoionisation of circumnuclear gas (Guainazzi & Bianchi 2006). Let us assume an ionised cone geometry as for NGC 1068 (see Kinkhabwala et al. 2002). The lack of warm absorption in Mrk 590 implies that our line of sight does not intersect warm gas, or that the gas in the line of sight is fully ionised and therefore it does not imprint absorption features. Thanks to this "clean" line of sight, we can see the scattering gas responsible for line emission in Seyfert 2 in this Seyfert 1 galaxy. The observed *EW* of the emission lines in Mrk 590 are weaker than in Seyfert 2 because we are directly observing the active nucleus and because the lines are diluted by the X-ray continuum. This scenario provides yet another confirmation of the Sy1/Sy2 dichotomy to be due to orientation effects.

Table 4. List of the serendipitous sources detected in the field of view of *Chandra* (Sources A, B, C) and *XMM-Newton* (Source B and C). Source B is already known as 1WGA J0214.5-0042.

Source	RA	Dec	Flux (0.3–10 keV)
–	–	–	($\times 10^{-14}$ erg cm^{-2} s^{-1})
A	02h 14m 34.0s	–00h 45m 58s	$2.88^{+2.5}_{-1.8}$ (ACIS)
B	02h 14m 34.7s	–00h 42m 43s	$26.7^{+0.9}_{-0.8}$ (MOS-2)
C	02h 14m 36.4s	–00h 42m 58s	$2.68^{+0.42}_{-0.38}$ (MOS-2)

5. Analysis of the serendipitous X-ray sources in the field of view

Besides the main target of these two observations, we have also studied three X-ray sources detected in the field of view of the *XMM-Newton* and *Chandra* images. For clarity, they will be referred to as Sources A, B and C. Table 4 lists their positions and fluxes.

Source A is visible only in the *Chandra* image at ∼7 arcsec northwest of the nucleus, thanks to the high spatial resolution of the satellite. Figure 10 shows the contour levels of the emission in the soft X-ray band and in the hard X-ray band, where Source A seems to be stronger. The ACIS spectrum

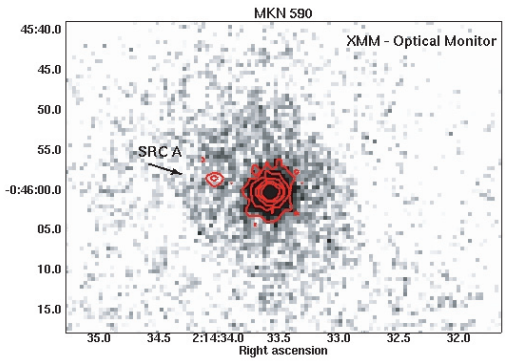

Fig. 11. XMM-Optical Monitor image in the *UVW*1 filter of Mrk 590 with Chandra contours overlapped. The image has been co-aligned with the one obtained by Chandra in order to take into account the different astrometry errors of the two instruments. As shown, no counterpart is evident for Source A.

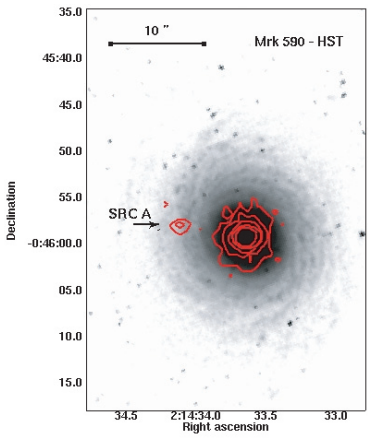

Fig. 12. HST image of Mrk 590 obtained in 1995. The overlapped contours mark the X-ray emission from Chandra. At the position of Source A no point source appears to be present. The X-ray source seems to be located within the extension of the galaxy and this may be favouring the hypothesis that Source A could be identified as a ULX in the galaxy. The HST and Chandra images have been co-aligned at the position of the X-ray nucleus.

was extracted yielding 46 counts in the 0.3−10 keV. When it is fitted with a power law and Galactic absorption, the photon index is found to be $\Gamma = 1.13 \pm 0.5$. The observed 0.3−10 keV flux is $\sim 2.88 \times 10^{-14}$ erg cm^{-2} s^{-1}, corresponding to a luminosity of about 4.3×10^{40} erg s^{-1} if the source is at the same redshift of Mrk590. We have searched in the OM images if any possible optical/UV counterpart is visible. There is no clear excess at the source position in any of them. From the position of the *Chandra* contours overlapped the *UVW*1 image (Fig. 11), we can deduce that Source A seems located in the host galaxy. We also have searched for archival images of Mrk 590 obtained by the Hubble Space Telescope: Fig. 12 shows Mrk 590 as observed by the Wide Field Planetary Camera 2 (WFPC2) with the filter *F606W* applied. The observation was performed on June 24th 1995 for 500 s. Figure 12 shows the *Chandra* contours overlapped to the optical image and although no optical counterpart is clearly visible, the location of Source A indicates that it could be an Ultra-Luminous X-ray source (ULX) in the spiral arms of Mrk 590. If the identification were confirmed, Source A represents a fairly typical ULX, although it must be noted that only a few ULX of those catalogued and studied so far exceed luminosities of $3-4\times10^{40}$ erg s^{-1} (Liu & Mirabel 2005; Miniutti et al. 2006).

Another possibility for the origin of Source A is that it could be a background AGN. Assuming that the present field is characterised by the same number of expected X-ray sources within a given area as observed by the deep *XMM-Newton* observation of the Lockman Hole, we can estimate the probability of Source A to be an AGN from the Lockman Hole Log N−Log S (Hasinger et al. 2001). According to the Log N−Log S, at fluxes equal or higher than 5×10^{-15} erg cm^{-2} s^{-1} in the 0.5−2 keV band, (corresponding to Source A flux), 200 X-ray sources per square degree are expected. Considering a circular area of radius equal to the distance of Source A from Mrk 590 (∼7.3 arcsec), the number of expected X-ray sources is 0.002 in an area of 1.256×10^{-5} deg^2. The use of the hard X-ray flux yields a similar estimate, i.e. 0.001 for the same area. These numbers indicate that the probability for Source A to be a background AGN is small but not null and therefore the origin of this source remains open.

Source B and Source C are visible in the EPIC-pn image of the field of view, but the exact positions are taken from *Chandra*, where the sources are clearly separated. We have found two possible optical counterparts in the Digitized Sky Survey, where the two sources appear extremely faint. Source B was already known as 1WGA J0214.5-0042, detected by ROSAT in the soft

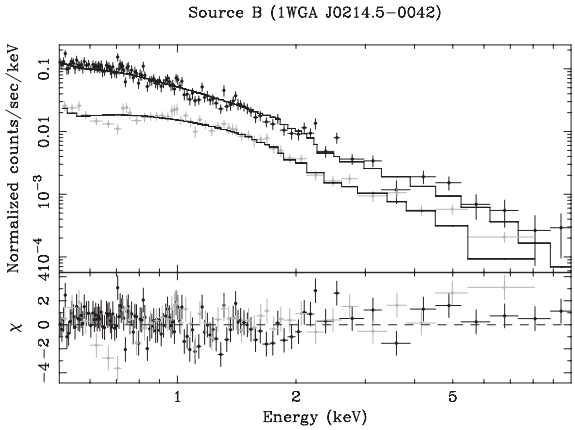

Fig. 13. Pn (black points) and MOS-2 (grey points) data of Source B (1WGA J0214.5-0042). The spectra in the top panel are fitted with a power law of $\Gamma \sim 2.4$ and the bottom panel shows the residuals of this fit.

X-rays (White et al. 2000). We have searched if the source is present in other catalogues or if other observations in different wavelengths are available, but only ROSAT has detected this source. Unfortunately, Source B falls just out of the field of view of the OM because of the orientation of the telescope, and out of the field of view of the MOS-1 because of the choice of the small window mode. Therefore, only the X-ray data from the pn and MOS-2 can reveal something on the nature of this source. The *XMM-Newton* spectrum is shown in Fig. 13. We have fitted pn and MOS-2 together with a power law and Galactic absorption towards the direction of Source B. The resulting photon index in the range 0.5−10 keV is quite steep, $\Gamma = 2.39 \pm 0.05$ with χ^2/d.o.f. = 415/356. The fluxes are $1.71 \pm 0.05 \times 10^{-13}$ erg cm^{-2} s^{-1} in the 0.3−2 keV and $9.55^{+0.32}_{0.51} \times 10^{-14}$ erg cm^{-2} s^{-1}. If the data are instead fitted with a broken power law with break energy $E = 2$ keV, the slopes are $\Gamma_{0.3-2} = 2.48 \pm 0.05$ and $\Gamma_{2-10} = 1.89 \pm 0.15$.

Source C is not present in any catalogue. The spectra extracted from the pn and MOS-2 and fitted with a power law and Galactic absorption yield $\Gamma = 2.02 \pm 0.23$, in the 0.5−10 keV range. The observed soft X-ray flux is

about 1.23×10^{-14} erg cm^{-2} s^{-1} and the hard X-ray flux is 1.47×10^{-14} erg cm^{-2} s^{-1}.

The lack of optical counterparts and other multiwavelength information on Sources B and C make it very difficult to understand the nature of these sources. It is clear from the spectral fitting and the different photon index that the two sources are distinct and not related to each other. Moreover as said above, they appear clearly separated in the *Chandra* image. Taking into account that in both sources the spectra are well fitted by a steep power law, the most likely interpretation for both of them is in terms of a background AGN.

6. Summary

The analysis of the simultaneous *XMM-Newton/Chandra* observation of the Seyfert 1 galaxy Mrk 590 has been presented. In the following the main results of this work are summarised:

- The analysis of the X-ray data reveals a fairly typical Sy1 spectrum. The broad-band continuum is well described by a power law with $\Gamma \sim 1.7$, a cold reflection component originating in distant matter and a blackbody with temperature $kT \sim 0.1$ keV.
- The iron K complex composed by 3 emission lines at ∼6.4, 6.7 and 7 keV has been clearly detected in the EPIC data. The width of the 6.4 line is resolved in both *Chandra* and *XMM-Newton* spectra with velocities in the range of 4−5000 km s^{-1}. The line is interpreted as being originated via reflection onto the torus-shaped material surrounding the active nucleus, although an origin in the BLR cannot be excluded.
- The two Fe lines at higher energies are consistent with being emitted by photoionisation of FeXXV and FeXXVI. The analysis of the high resolution data highlighted the presence of an OVIII Lyα emission line consistent with being emitted in the same photoionised gas. The observation of highly ionised emission lines with no absorption from warm gas is interpreted as an orientation effect: the nucleus is surrounded by warm scattering clouds, but it is seen along a particular line of sight with either fully ionised material or no intervening material at all.
- The OM measurements of the UV fluxes are found to be above the extrapolation of the X-ray spectrum, suggesting the presence of a UV bump.
- Three serendipitous sources are present in the field of view of *Chandra* (Sources A, B, C) and *XMM-Newton*/EPIC-pn (only Sources B and C). All of them are characterised by X-ray power laws and fluxes typical of AGN. With regard to Source A, the location and the estimated luminosity of the source (assuming it belongs to Mrk 590), may induce us to interpret it as a ULX source, although no counterparts are observed in the optical and ultraviolet data.

Acknowledgements. This paper is based on observations obtained with *XMM-Newton*, an ESA science mission with instruments and contributions directly funded by ESA Member States and NASA. We would like to thank the Chandra X-ray Center and the anonymous referee for helpful comments on this publication.

References

Antonucci, R. 1993, ARA&A, 31, 473
Behar, E., Rasmussen, A. P., Blustin, A. J., et al. 2003, ApJ, 598, 232
Bianchi, S., Matt, G., Balestra, I., & Perola, G. C. 2003a, A&A, 407, L21
Bianchi, S., Balestra, I., Matt, G., Guainazzi, M., & Perola, G. C. 2003b, A&A, 402, 141
Bianchi, S., Matt, G., Balestra, I., Guainazzi, M., & Perola, G. C. 2004, A&A, 422, 65
Bianchi, S., Matt, G., Nicastro, F., Porquet, D., & Dubau, J. 2005, MNRAS, 357, 599
Blustin, A. J., Branduardi-Raymont, G., Behar, E., et al. 2003, A&A, 403, 481
Boller, T., Brandt, W. N., & Fink, H. 1996, A&A, 305, 53
Cardelli, J. A., Clayton, G. C., & Mathis, J. S. 1989, ApJ, 345, 245
Canizares, C. R., Davis, J. E., Dewey, D., et al. 2005, PASP, 117, 1144
Cash, W. 1976, A&A, 52, 307
Crummy, J., Fabian, A. C., Gallo, L., & Ross, R. R. 2006, MNRAS, 365, 1067
den Herder, J. W., Brinkman, A. C., Kahn, S. M., et al. 2001, A&A, 365, L7
Dickey, J. M., & Lockman, F. J. 1990, ARA&A, 28, 215
Fabian, A. C., Iwasawa, K., Reynolds, C. S., & Young, A. J. 2000, PASP, 112, 1145
Gabriel, C., Denby, M., Fyfe, D. J., et al. 2004, ASPC, 314, 759
George, I. M., & Fabian, A. C. 1991, MNRAS, 249, 352
Gallo, L. C., Lehmann, I., Pietsch, W., et al. 2006, MNRAS, 365, 688
George, I. M., Turner, T. J., Netzer, H., et al. 1998, ApJS, 114, 73
Ghisellini, G., Haardt, F., & Matt, G. 1994, MNRAS, 267, 743
Gierliński, M., & Done, C. 2004, MNRAS, 349, L7
Guainazzi, M., & Bianchi, S. 2006, On the origin of soft X-rays in obscured AGN: answers from high-resolution spectroscopy with XMM-Newton [arXiv:astro-ph/0610715]
Haardt, F., & Maraschi, L. 1993, ApJ, 413, 507
Hasinger, G., Altieri, B., Arnaud, M., et al. 2001, A&A, 365, L45
Kinkhabwala, A., Sako, M., Behar, E., et al. 2002, ApJ, 575, 732
Jiménez-Bailón, E., Piconcelli, E., Guainazzi, M., et al. 2005, A&A, 435, 449
Kaastra, J. S., Mewe, R., Liedahl, D. A., Komossa, S., & Brinkman, A. C. 2000, A&A, 354, L83
Kaspi, S., Brandt, W. N., Netzer, H., et al. 2001, ApJ, 554, 216
Kriss, G. A., Canizares, C. R., & Ricker, G. R. 1980, ApJ, 242, 492
Liu, Q. Z., & Mirabel, I. F. 2005, A&A, 429, 1125
Longinotti, A. L., Cappi, M., Nandra, K., Dadina, M., & Pellegrini, S. 2003, A&A, 410, 471
Magdziarz, P., & Zdziarski, A. A. 1995, MNRAS, 273, 837
Malizia, A., Bassani, L., Zhang, S. N., et al. 1999, ApJ, 519, 637
Mason, K. O., Breeveld, A., Much, R., et al. 2001, A&A, 365, L36
Matt, G., Bianchi, S., de Rosa, A., Grandi, P., & Perola, G. C. 2006, A&A, 445, 451
Miniutti, G., Ponti, G., Dadina, M., et al. 2006, MNRAS, 373, L1
Molendi, S., Bianchi, S., & Matt, G. 2003, MNRAS, 343, L1
Nandra, K. 2006, MNRAS, 368, L62
Nandra, K., George, I. M., Mushotzky, R. F., Turner, T. J., & Yaqoob, T. 1999, ApJ, 523, L17
Netzer, H., Lemze, D., Kaspi, S., et al. 2005, ApJ, 629, 739
Piccinotti, G., Mushotzky, R. F., Boldt, E. A., et al. 1982, ApJ, 253, 485
Piconcelli, E., Jimenez-Bailón, E., Guainazzi, M., et al. 2005, A&A, 432, 15
Ponti, G., Cappi, M., Dadina, M., & Malaguti, G. 2004, A&A, 417, 451
Reynolds, C. S. 1997, MNRAS, 286, 513
Ross, R. R., & Fabian, A. C. 2005, MNRAS, 358, 211
Smith, R. A. N., Page, M. J., & Branduardi-Raymont, G. 2006, The XMM-Newton RGS spectrum of the high luminosity Seyfert 1 galaxy Markarian 509 [arXiv:astro-ph/0609746]
Stirpe, G. M. 1990, A&AS, 85, 1049
Strateva, I. V., Brandt, W. N., Schneider, D. P., Vanden Berk, D. G., & Vignali, C. 2005, AJ, 130, 387
Strüder, L., Briel, U., Dennerl, K., et al. 2001, A&A, 365, L18
Turner, T. J., & Pounds, K. A. 1989, MNRAS, 240, 833
Turner, T. J., Mushotzky, R. F., Yaqoob, T., et al. 2002, ApJ, 574, L123
Yaqoob, T., & Padmanabhan, U. 2004, ApJ, 604, 63
White, N. E., Giommi, P., & Angelini, L. 2000, yCat, 9031, 0